Chapter

AUTONOMOUS SOLAR PV/WIND/REGENERATIVE HYDROGEN FUEL CELL ENERGY STORAGE SYSTEM FOR CELL TOWERS– DOUBLES AS MICRO-GRID.

Gerard Jansen[a], Zahir Dehouche[a], Harry Corrigan[b], Richard Bonser[a]

[a] College of Engineering, Design and Physical Sciences, Brunel University London, UK

[b] SolarBotanic Ltd., London, UK

ABSTRACT

Mobile telephone penetration has a significant impact on growth in both the upper-low-income and the low-income countries in Africa and therefor reliable power is critical. A large number of telecommunication base stations operate on unreliable grid or no grid at all, and rely on batteries or diesel generators for primary or back-up power. This work proposes an autonomous renewable energy micro-grid, using Solar Photovoltaics and Wind Turbine to generate electricity, and a Regenerative Hydrogen Fuel Cell as energy storage system for up to 10 days. The system is validated using MATLAB/Simulink software and real-life weather data and optimized for a 25kW micro-grid near Dakar, Senegal. The simulations show a smart load-following system that instantaneously recognizes the most cost effective source of electricity to power the load. The optimized energy system consist of 20,000 kWh of hydrogen stored in AB2 Ti-based alloys. Levelised Cost of Electricity based on the outcomes of the MATLAB/Simulink model show the economic potential of an RHFC as back-up for micro-grids, allowing affordable and reliable electricity to rural areas in developing countries, with a LCOE of

10.17 ¢/kWh, RHFC is the most cost effective back-up for this application. However, the system is highly influenced by local climate; hence the LCOE and system sizing should be individually configured based on the geographical location of the planned deployment.

Keywords: Hydrogen, Fuel Cell, Micro-Grid, Renewable, Energy, Electrolysis, Storage, Metal-Hydride, Wind, Solar Photovoltaics

INTRODUCTION

Failure to climate change mitigation and adaption is one of the biggest global risks according to the World Economic Forum's multistakeholder communities [1].The increased awareness of the risks of climate change leads to a shift in investment from fossil fuels towards renewable energy sources like wind and solar photovoltaics (PV). Despite the global new investment in renewables falling back to $241.6 Billion, the lowest since 2013, installation of renewable power capacity worldwide hits a record high, growing at more than twice the rate of demand [2]. There are two main reasons for the decline in investment in renewable energy during 2016. First, there was a slowdown in investment in some emerging markets such as Japan and China. In addition to this, there was a significant cost reduction in solar PV and in onshore and offshore wind power, which also improved the cost-competitiveness of these technologies [2].

The cost-competitiveness of solar PV and wind technologies can be seen in the declining Levelised Cost of Electricity. In some locations, solar PV and wind technologies have reached grid parity or even generate electricity cheaper than fossil fuels. The forecasts for the future are even brighter: By 2040, LCOE for Solar PV drops by 66% by 2040, onshore wind drops by 47% and offshore wind drops by 71% by 2040 [3].

The increase installed capacity of renewable energy sources brings its specific challenges in both developed and developing countries because of the intermittence of energy generation. In developed countries where renewable energy sources are connected to an electricity grid, fossil fuel power plants have to support the intermittent renewables. With the increased amount of renewables connected to the grid, a point will be reached where fossil fuel power plants cannot turned down any more and solar PV and wind farms have to reduce or stop their generation. When the renewable generation then drops, fossil fuel power plants have to ramp up their generation. This phenomenon is represented in the Californian Duck Curve, where the net load (total energy demand minus solar PV generation) is plotted. A 13,000 MW ramp is predicted in 2020 at the end of the

afternoon when the sun sets and the energy demand is highest [4]. In 2016, an actual ramp of 10,892 MW was measured, more then expected and arguably showing that the ramp might be even steeper then the 13,000MW predicted [5].

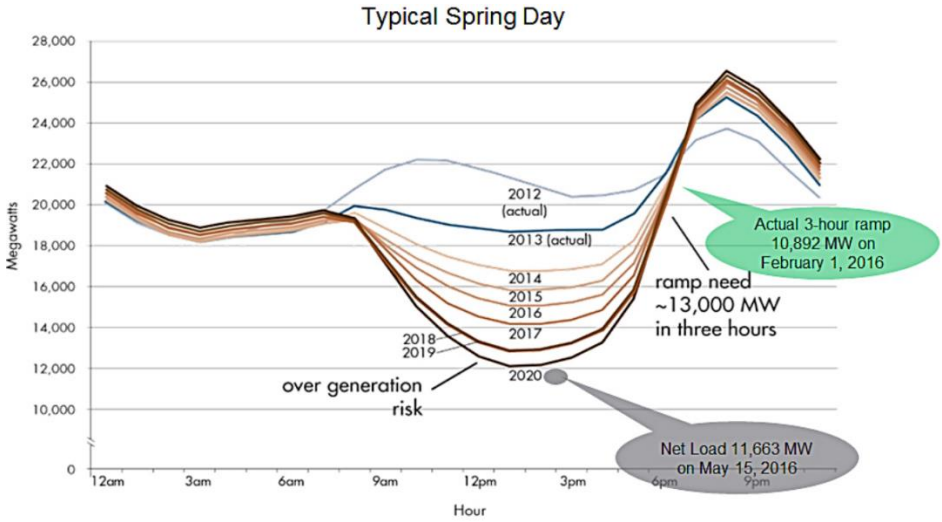

Figure 1: The California Duck Curve shows steep ramping needs and overgeneration risk [5]

In developing countries and remote areas, where there is no (reliable) grid connection, the challenges and opportunities are even bigger. Worldwide, almost 1.1 billion people are living without electricity [6]. In addition to that, in developing countries, diesel generators are often used for electricity production and come with environmental, health and cost concerns. Electricity is fundamental for many essential services that increase income in rural areas such as; agriculture, clean drinking water, health care, education, communications, and quality of life [7]. It is critical for developing countries to have access to cheap, reliable electricity and give them the opportunity to leap-frog towards modern energy generating technologies in order to mitigate environmental issues.

Reliable electricity is also important for the cell phone tower operators to serve their customers with an uninterupted network. Mobile telephone penetration has a significant impact on growth in both the upper-low-income and the low-income countries in Africa [8]. Deploying reliable communication infrastructure is key to allow developing countries to develop and can be achieved by sharing knowledge of technologies with these countries. The increase in cell phone penetration has led to an increase of energy consumption of cell phone towers.

Limited grid availability combined with inadequate electricity supply capacities has forced mobile operators to rely on alternative power sources such as diesel generators, both on-grid and off-grid [9]. Nowadays, over 75% of cell phone towers in Nigeria rely on Diesel generators or batteries for reliable power supply. Concerns of diesel costs, regular maintenance, theft, and environmental issues have raised the attention of deploying renewable energy technologies [9] [10]. GSMA has estimated that 10,890 sites in Nigeria and Ghana alone could convert to green power deployments [11].

The ultimate goal of this project is to design, test and analyse a Regenerative Hydrogen Fuel Cell (RHFC) system for back-up applications of Renewable Energy Technologies deployed on existing cell phone tower structures to reduce initial investment and replace polluting diesel generators. The proposed system contains of a water electrolyser, where the excess electricity from renewable sources is used to split water into hydrogen and oxygen. The hydrogen is then stored in a sorption Solid-Hydrogen Energy Storage Cell. This technology has the advantage of low pressure and low temperature storage operation, eliminating the need for hydrogen compression and hence lowering parasitic system losses. The Solid-Hydrogen Energy Storage Cell has negligible self-discharge allowing energy storage for long periods and can therefore be used for seasonal shifting. Thereby, hydrogen offers much higher storage potential than other technologies [12]. When electricity generated from the renewable sources is not sufficient to power the load, a Polymer Electrolyte Membrane Fuel Cell (PEMFC) is used to generate electricity from hydrogen, with only water and heat as by-products.

This study shows the design of the integrated RHFC system with performance simulations in MATLAB/Simulink. First, the individual key components of the system are explained and the key parameters for each system are discussed. Each of the components can be individually modelled and coupled together using MATLAB/Simulink. The control system will be discussed individually and shows the decision making of the smart energy system.

Following that, results from the simulation of the optimized energy system are used to calculate the Levelised Cost of Electricity (LCOE). The Levelised Cost of Electricity is an important financial parameter to measure cost-effectiveness of energy generating technologies. Although LCOE calculations are highly sensitive to the underlying data, it offers a comparison between projects and technologies. The LCOE of the integrated system will be compared to that of conventional diesel generators and lithium-ion battery packs.

The ultimate goal of the energy system is to establish a smart, reliable, flexible, adaptative, sustainable and load-following energy storage and generation system which can boost availability of cell phone signal and electricity in general,

allowing for an improvement in quality of life for developing countries. With renewable energy generation being very dependend on the geographical location where the system is deployed, the system sizing is compared for several microgrid scenarios and compared to other back-up technologies e.g. diesel gensets and batteries.

METHODS

System design

To validate the characteristics of the system, such as ability to follow the load and storage capacity, a Simulink model is made. In this model, the RHFC unit is coupled to a Solar PV array and Wind Turbine. This model helps selecting the operation characteristics of the control system and helps size the system based on the local climate and load requirements. The Simulink model is set up respecting the technologies' characteristics. Before the MATLAB/Simulink model can be made, initial system design is required to identify the relevant technologies and characteristics involved.

The stand-alone system is designed for autonomous use, where hydrogen is generated and used on-site to avoid transportation emissions and import issues. The system consists of several sub-systems: Solar PV and Wind Turbine for renewable energy generation, an Electrolyser to convert surplus of electricity into hydrogen, a Hydrogen Energy Storage System, a Fuel Cell for energy conversion of hydrogen into electricity and a smart control system that has the potential to be interfaced to the Internet of Energy (IoE).

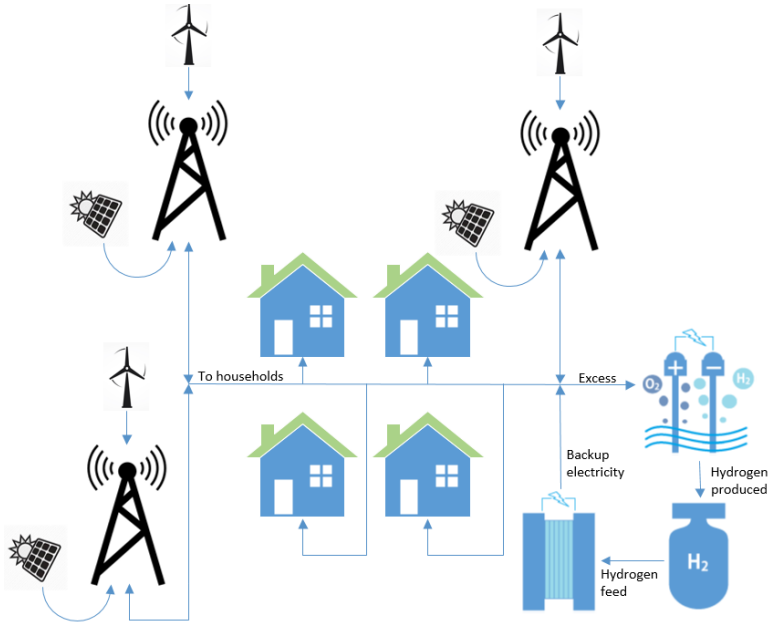

Figure 2: Schematic overview of a decentralized renewable energy micro-grid with hydrogen back-up

A Regenerative Hydrogen Fuel Cell system is designed with the aim of limiting parasitic losses by recycling waste heat. The electrolyser is designed to be powered by the excess electricity of renewable energy sources. Once renewable energy sources are not sufficient to power the load, the fuel cell starts. In this scenario, the electrolyser and fuel cell will never run at the same time, therefore, two operation scenarios are possible as is schematically displayed in Figure 3.

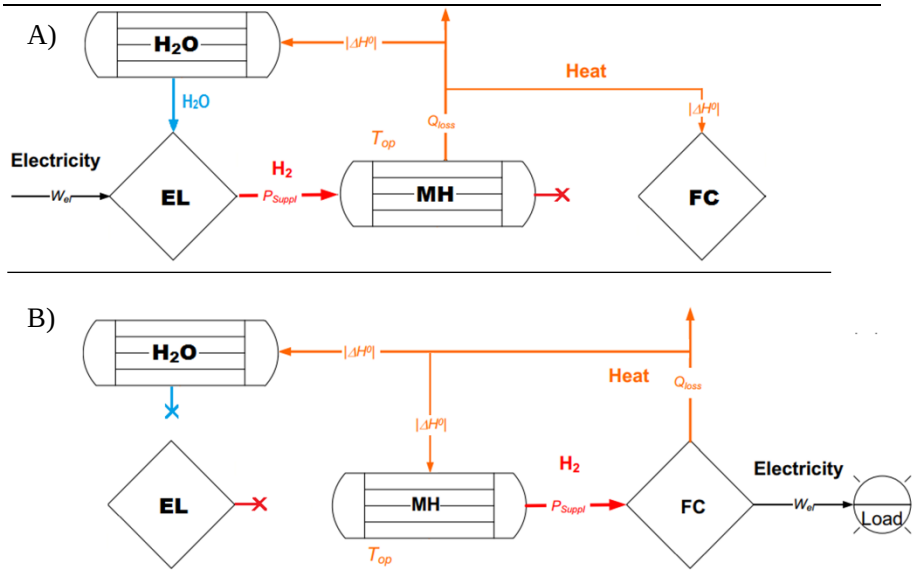

Figure 3: Schematic design of heat recovery in a regenerative hydrogen fuel cell system, where situation A represents the scenario where hydrogen is generated using excess electricity from the renewables and storing it in the Metal Hydride Hydrogen Storage Cell. Situation B represents the scenario where the Fuel Cell delivers electricity to the load.

In situation A), water and electricity are supplied to the electrolyser to produce hydrogen. Hydrogen is stored in the Metal Hydride Hydrogen Storage Vessel, inducing an exothermic reaction. The waste heat of the hydriding reaction is recovered by circulating water and used to pre-heat water that is fed to the electrolyser, as well as preheating the fuel cell stack for fast start-up. In situation B), heat is applied to start dehydriding the metal-hydride and gaseous hydrogen is fed to the fuel cell. Heat coming from the exothermic reaction in the fuel cell is recovered by keeping the metal-hydride at the right temperature, reducing electric heating requirements, as well as pre-heating the water stored to allow quick start up for the electrolysis.

Renewable energy system

Various renewable energy technologies can be implemented into a micro-grid. With the aim to integrate the renewable energy technologies directly on existing

cell phone tower sites and structures, Solar Photovoltaics and Wind Turbine are the choice to go.

Solar Photovoltaics and Wind Turbines rely on the climatic data of the location of deployment. It is therefore critical to analyze this data in order to select the best components. Figure 4 shows the average monthly solar irradiance (W/m^2) and Temperature (°C) that influence the performance of the solar array, and the wind speed (m/s) at 40m height for wind turbine selection.

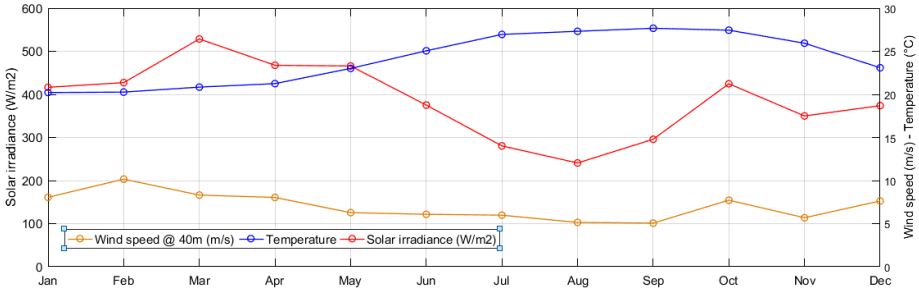

Figure 4: Climate data for Dakar International Airport, Senegal.

The data shows a relatively high potential for Solar PV, only dropping from June until August due to high percipitation in the rain season. Obviously, solar energy is not available all day around, as the sun sets in the evening. Therefore Solar PV array should be oversized to allow for excess energy generation for storage. However, wind speed is only slightly related to the time of the day due increase in temperature difference between the earths surface and the atmosphere. Therefore, during nightime, wind turbine still offer potential for energy generation as can be seen in Figure 5, and potentially reduce the installed capacity of storage, Solar PV, and /or electrolyser.

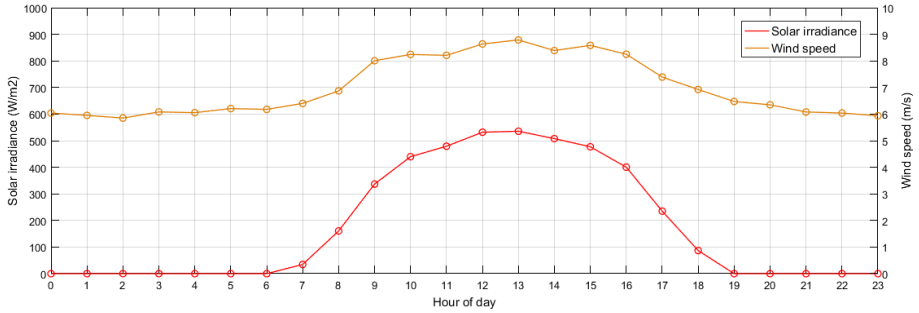

Figure 5: Average hourly solar irradiance (W/m^2) and wind speed at 40m (m/s)

Solar Photovoltaic (PV) cells use the photovoltaic effect to convert sunlight into electrical energy [13].The use of Solar PV cells is one of the major methods to harness energy from sunlight, without producing carbon dioxide, noise or any noxious gas [14].

PV cells structure consist of at least two layers of semiconducting material (e.g. silicon). One of the layers has a negative character (N-type layer), the other layer has the tendency to attract electrons (P-type layer). In between the two layers, a p-n junction is created [15].

Sunlight consists of photons. When a photon, with an energy that equals or exceeds the semiconductor bandgap energy of the p-n junction material, hits the cell, it is capable of creating an electron-hole pair. The electrons in the outer shell of the silicon atoms diffuse into the N-type layer and leaves a hole that diffuses into the P-type layer [16]. Electrons are conducted by the front electrode and flow via an external electric circuit back to the back electrode, creating an electric current [17].

The current generated by a single Solar PV module depends on the temperature of the solar cell and the solar irradiance and the amount of cells connected in series and parallel to form a module. Connecting multiple modules in series or parallel creates an array. The current transferred to the load by the PV module is determined from [18]:

$$I_{PV} = N_P I_{PH} - N_P I_0 \left[exp\left(\frac{\frac{V}{N_S} + IR_S}{nV_T} \right) - 1 \right] - N_P I_{SH} \qquad (1)$$

Where, N_P is the number of cells in parallel, I_{PH} is the cell photo-current (A), I_0 is the dark saturation current (A), V is the operating Voltage (V), N_S is the number of cells in series, I is the cell operating current (A), R_S is the series resistance (Ω), n is the ideality factor of the diode (1.2), V_T is the thermal voltage (V), and I_{SH} is the shunt current (A), which is expressed as:

$$I_{SH} = \frac{\frac{V}{N_S} + IR_S}{R_{SH}} \qquad (2)$$

The dark saturation current varies with the cell temperature and is found by:

$$I_0 = I_{RS}\left[\frac{T}{T_{ref}}\right]^3 exp\left[\frac{qE_{g0}}{nk}\left(\frac{1}{T}-\frac{1}{T_{ref}}\right)\right] \quad (3)$$

Where, $I_{RS}$is the module reverse saturation current (A), T is the operating temperature (K), T_{ref} is the reference temperature (298.15 K), E_{g0} is the band gap energy of silicon semiconductor (1.1 eV), q is the electron charge ($1.6 \cdot 10^{-19}$C), and k is the Boltzmann's constant ($1.3805 \cdot 10^{-23}$ J/K).

The thermal voltage is found by:

$$V_T = \frac{kT}{q} \quad (4)$$

The module photo-current is found by:

$$I_{PH} = I_{SC} + K_i(T - T_{ref}) \cdot \frac{G}{1000} \quad (5)$$

Where, I_{SC} is the short-circuit current of the cell at operating conditions (6.48 A for selected module), K_i is the short-circuit current at Standard Testing Conditions, and G is the solar irradiance (W/m^2).

The cell reverse saturation current is found by:

$$I_{RS} = \frac{I_{SC}}{\left[exp\left(\frac{qV_{OC}}{N_S nkT}\right) - 1\right]} \quad (6)$$

Where, V_{OC} is the cell open circuit voltage (0.68 V for selected cell).

Wind Turbines work on the principle of movement of air. Kinetic energy carried by the wind can be captured and converted into mechanical or electrical energy by use of a wind turbine. The motion in the air generates a rotational movement in a gearbox or motor, which transfers this movement via a shaft to a generator to generate electrical energy. The average kinetic power in the wind can be expressed as:

$$P_{avg} = \frac{1}{2}\rho A(V^3)_{avg} \quad (7)$$

Where, ρ is the density of air (1.225 kg/m^3), A is the area of the rotor (m^2), and V_W is the wind speed at hub height (m/s). As is seen in equation 7, the power generated is largely influenced by the wind speed. Wind speed is usually not measured at the height of the wind turbine, as simulation require this input before construction of the wind turbine. Wind speed measured at a reference height close to the planned location of the wind turbine can be adjusted to the hub height of the wind turbine. The wind speed is adjusted by:

$$V_W = V_{ref}\left(\frac{H}{H_{ref}}\right)^{\alpha} \tag{8}$$

Where, V_{ref} is the reference wind speed (m/s), H is the hub height (40 m), H_{ref} is the height at which V_{ref} is measured (10 m), and α is an empirically derived coefficient that varies dependent upon the stability of the atmosphere conditions (0.14 for selected location).

To determine the power captured from the wind by the wind turbine, the wind turbine's rotor power coefficient and the electrical and mechanical efficiencies of the wind turbine should be taken into account as expressed in equation 9:

$$P = \frac{1}{2}\rho A V_W^3 C_p \eta_{mech}\eta_{elec} \tag{9}$$

Where, C_p is the rotor power coefficient which depends on the design of the wind turbines airfoil, η_{mech} is the conversion efficiency of mechanical power in the rotor to electrical power in the generator axis, and η_{elec} encompasses the electrical efficiency of the generator, frequency converter, transformer etc.

Wind speed is always fluctuating, hence the energy content of the wind is always changing according to equation 7. The wind speed characteristics is the most critical parameter to evaluate the potential energy generation at the selected site. The wind speed variation can be described by a probability distribution function which expresses the probability of a wind speed occurring based on the recorded fraction of hours per year at set wind speed. The average wind speed can then be expressed as:

$$V_{avg} = \sum_i [V_i \cdot (fraction\ of\ hours\ @\ V_i)] \tag{10}$$

The wind speed variation found from equation 4 are best described by the Weibull probability function:

$$f(V)_{Weibull} = \frac{k}{c}\left(\frac{V}{c}\right)^{k-1} \exp\left[-\left(\frac{V}{c}\right)^{k}\right] \tag{11}$$

Where shape parameter k indicates how the wind speeds are distributed and the scale parameter c indicates how windy the site is. The most realistic wind turbine site is found when the shape parameter $k = 2$. In this case, the probability density function is called Rayleigh probability density function:

$$f(V)_{Rayleigh} = \left(\frac{\pi \bar{V}}{2\bar{V}^2}\right) \exp\left[-\frac{\pi}{4}\left(\frac{V}{\bar{V}}\right)^2\right] \tag{12}$$

The power density distribution of the selected site is obtained by multiplying the specific power produced at each wind speed by the probability of occurrence of each wind speed:

$$\frac{P}{A} = \frac{1}{2}\rho V_W^3 f(V) \tag{13}$$

The power captured from the wind and converted into electrical power can be found by equation 14 for Weibull winds and equation 15 for Rayleigh winds:

$$P = \frac{1}{2}\rho A V_W^3 \eta \tag{14}$$

$$P = \frac{6}{\pi} \cdot \frac{1}{2}\rho A V_W^3 \eta \tag{15}$$

Where, η is the overall efficiency, which includes the capacity factor, mechanical efficiency and electrical efficiency of the generator. Energy generated by the wind and solar renewable energy technologies is first used to power the load, any excess energy is used to generate hydrogen using an electrolyser.

Electrolyser system

Hydrogen is the most abundant element on earth and makes up for more than 90% of all the atoms. It was first recognized by Henry Cavendish in 1776 and

thanks its name to the Greek words hydro (water), and genes (forming) [19]. Although hydrogen is very abundant on earth, it is barely available as a pure hydrogen gas. Pure hydrogen is so light that it will gain enough velocity from collisions with other gases that it will quickly escape the earth's atmosphere [19].Since hydrogen is bond with other elements, it can be seen as a secondary energy source, meaning hydrogen is an energy carrier and not a fuel. By use of a fuel cell it can be converted into a fuel. To unleash the maximum amount of energy from hydrogen, pure hydrogen gas should be induced in the fuel cell anode in order to provide a high energy conversion efficiency and prevent from excessive degradation.Hence, hydrogen is to be split from other elements to produce useful gas.

Available hydrogen is mainly bond with other elements such as water (H_2O) and organic compounds matter such as living plants, petroleum and coal [20]. The main routes to pure hydrogen production are steam reforming and electrolysis. Steam reforming process is a two-stage process, where methane is split to produce hydrogen [21]. Although steam reforming is a relatively cheap way to produce hydrogen, it offers low purity hydrogen with a high concentration of carbonaceous species such a carbon monoxide (CO). In addition to this, hydrogen is split from a fossil fuel, hence it does not replace dependencies on fossil fuels [22].

Generation of high purity hydrogen without greenhouse gas emissions can be achieved by water electrolysis. The electrolysis process splits water into hydrogen and oxygen through the application of electrical energy, hence electrolysis is more suited for micro-grid or grid-balancing applications as it can be coupled to intermittent renewable energy sources. The goal of DOE is to reduce costs of distributed hydrogen production by electrolysis to below \$4/kg H_2 by 2020 [23]. Current costs of hydrogen production differ per electrolysis technology used and the (renewable) electricity source.

CO_2 emissions depend on the source of electricity but with electricity produced from renewable energy sources (e.g. wind energy), global warming potential can drop as low as 0.68 kg CO_2 eq. /kg H_2 [24].

Electrolysis technologies

Over the years, many ways of producing hydrogen using electrolosis have been developed. Main technologies used for electrolysis today are alkaline membrane, polymer electrolyte membrane (PEM), and anion exchange membrane (AEM) electrolysis cells. To find the most suitable electrolysis technology for application in an on-site regenerative hydrogen energy storage system, the three mentioned technologies are critically analysed and compared.

Alkaline electrolysis commonly uses nickel- and cobalt-based oxides in respectively the anode and cathode, with a 30-40% KOH liquid electrolyte [25]. Since electrolysis was discovered by Troostwijk and Diemann in 1789, alkaline electrolysis has become a well-matured technology and is the most extended technology for electrolysis at a commercial level worldwide. The advantage of this technology is the absence of noble metal catalyst materials allowing a low cost system. However the purity of the delivered hydrogen is relatively low due to amine contamination in the hydrogen stream.

In PEM electrolysis, the anode and cathode usually consist of platinum nanoparticles supported by high surface area carbon. The Polymer Electrolyte Membrane is a solid electrolyte, typically Nafion®, and conducts only hydrogen protons (H^+). PEM electrolysers can run at high current density and allow a wide range of operation, making them favourable for the intermittent renewable energy generation.

Anion exchange membrane electrolysis offers the advantages of both the PEM and Alkaline electrolysis. However, lack of knowledge on membrane and catalyst stability limit the maturity of AEM electrolysis and hence, only a limited amount of commercial available system is available.

Table 1: Typical specifications of alkaline, PEM, and AEM electrolyser systems, data compiled and modified from [25] [26] [27]

	Alkaline	PEM	AEM
Nominal cell efficiency (%)	60-70	70-80	60-70
Operating temperature (^oC)	60-80	40-80	50-70
Operating pressure (Bar)	< 30	30 - 80	≈ 30
Current density (A/cm2)	0.2 - 0.4	0.6 - 2.0	0.1 - 0.7
Cell voltage (V)	1.8 - 2.4	1.8 - 2.2	1.8 - 2.2
Specific energy (kWh/Nm3)	4.5 - 7.0	4.5 - 7.5	4.8 - 5.2
Lifetime stack (h)	< 90.000	> 50.000	N/A
Purity of Hydrogen (%)	< 99.9	≈ 99.999	≈ 99.99
Cold start up time (min)	≈ 15	< 15	< 15

Principles of Polymer Electrolyte Membrane Electrolysis

As PEM electrolysis is the favourable technology to use in a hydrogen based micro-grid, full understanding of the technology and its controls is required.

A schematic representation of PEM electrolysis is given in Figure 6. Pre-heated water enters the anode side of the PEM electrolysis cell. When a Direct Current (DC) power source (e.g. from Solar PV) is applied, hydrogen molecules are split from the oxygen molecule and lose their electrons simultaneously due to the DC power source acting on the cell. The hydrogen protons (H^+) are conducted through the PEM, excess water is recirculated to the water reservoir, and oxygen is either vented out to safety or captured and stored in a pressurized tank. On the cathode side, hydrogen protons and electrons combine to form high-purity hydrogen gas.

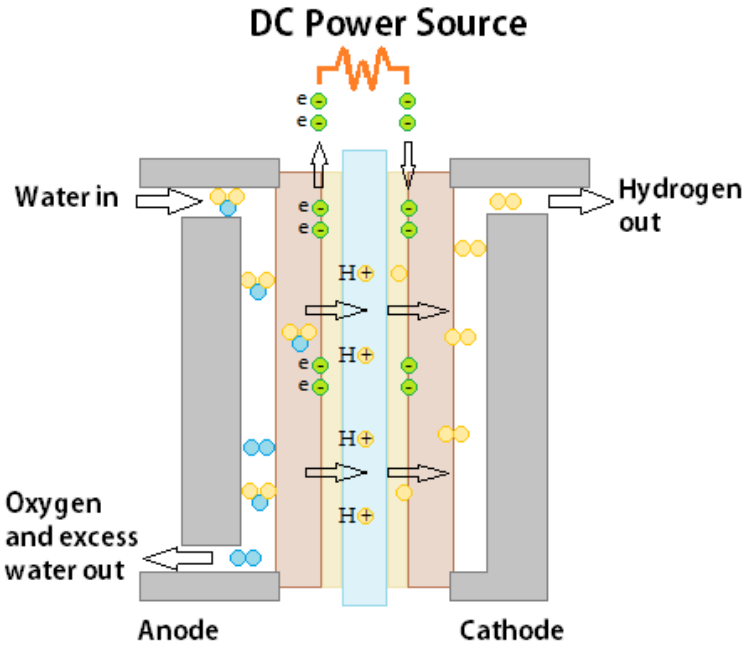

Figure 6: Schematic representation of Polymer Electrolyte Membrane water electrolysis

In PEM Electrolysis, DC electricity is applied to liquid water (H_2O) to split it into hydrogen (H_2) and oxygen (O_2) gases. Under Standard Temperature and Pressure (STP) conditions (1 atm and 25^{o}C), the minimum electrical energy required to start the electrolysis process is 237.2 kJ/mole of water and is referred to as the Gibbs' Free Energy (ΔG). Thereby, 48.6 kJ/mole of thermal energy is required to split one molecule of water [28].The correlating equation to this process is [22]:

$$2H_2O + Electricity + Heat \rightarrow 2H_2 + O_2 \quad (16)$$

Where electricity and heat depend on the operating conditions of the PEM electrolysis cell. According to Faraday's law of electrolysis, hydrogen production is directly proportional to the electric charge applied at the electrodes. The hydrogen production rate of a PEM electrolyser can therefore be expressed as:

$$f_{H_2} = \eta_f \frac{I}{nF} \quad (17)$$

Where f_{H_2} is the hydrogen production rate (mol/s), η_f is the Faraday efficiency of electrolysis, I is the electric current applied at the electrodes surface (A), n is the electrons transferred in the reaction (2 for hydrogen) and F is the Faraday constant (96,485 C/mol). The Faraday efficiency of electrolysis can be found by:

$$\eta_f = 96.5e^{(\frac{0.09}{i_e} - \frac{75.5}{i_e^2})} \quad (18)$$

The applied electrical current to the electrodes is directly related to irreversible losses in the electrolyser and will increase the stack voltage of the electrolyser as per:

$$V_{el} = V_{Nernst} + E_{act} + E_{ohm} + E_{conc} \quad (19)$$

Where, $V_{FC}$is the fuel cell voltage (V), $V_{ele}$is the electrolyser voltage (V), V_{Nernst} is the Nernst voltage (1.482V), E_{act} is the activation overpotential (V), E_{ohm} is the ohmic overpotential (V), and E_{conc} is the concentration overpotential.

The activation overpotential is found by:

$$E_{act} = -2.3\frac{RT}{\alpha F}\log(i_0) + \frac{RT}{\alpha F}\log(i) \quad (20)$$

Where, R is the universal gas constant (8,314 J kmol^{-1} K^{-1}), T is the operating temperature (K), α is the charge transfer coefficient (0.23), F is the Faraday's constant (96,485 A s mole^{-1}), i_0 is the exchange current density (4.5 x 10^{-2}A cm^{-2}), and i is the operating current density (A cm^{-2}).

The ohmicoverpotential is found by:

$$E_{ohm} = iR_i \tag{21}$$

Where, R_i is the cell internal resistance (0.21 Ω cm^{-2}). The concentration overpotential is found by:

$$E_{conc} = \frac{RT}{nF} \ln\left(\frac{i_L}{i_L - i}\right) \tag{22}$$

Where, i_L is the limiting current density (2.2 A cm^{-2}). Hydrogen generated by the electrolyser will be stored in a hydrogen energy storage system.

Hydrogen energy storage system

Hydrogen storage remains a challenge for integrated system design. At ambient temperature, one gram of hydrogen occupies a volume of 11 litres [29]. Therefore, storage of hydrogen faces challenges to make it economic, efficient and safe. The three mainly used techniques for hydrogen storage are high-pressure gas, cryogenic liquid and solid metal-hydride. Different technologies and materials used for hydrogen storage are presented in Figure 7.

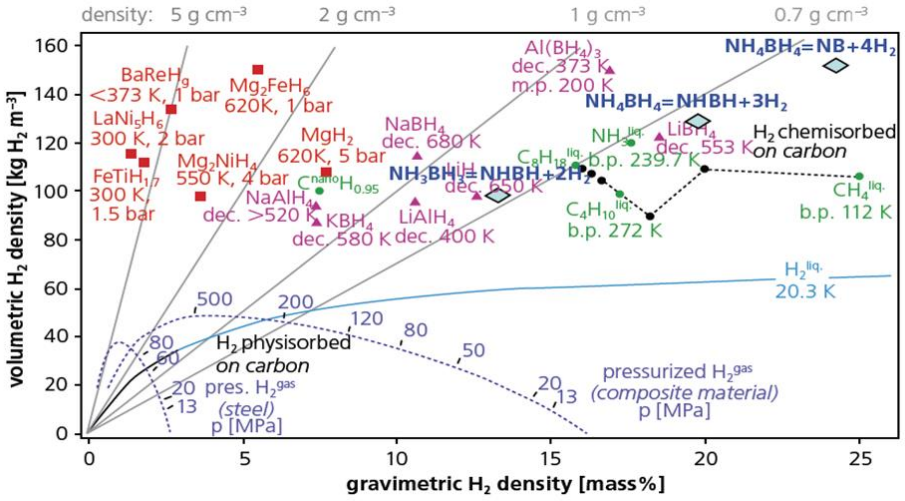

Figure 7: Gravimetric and volumetric hydrogen densities of some hydrogen storage systems [30]

Hydrogen storage technologies

High-Pressure Gas

Compressing hydrogen to a pressure of 350-700 bar reduces the space needed to store one kilogram of hydrogen drastically. Increasing the pressure from 1 bar to 350 bar increases the hydrogen density from 0.089 g/L to 22.9 g/L [31]. Compressing further to 700 bar increases the density to 39 g/L [32]. Due to the chemical properties of hydrogen and the high pressures required, sophisticated piston-type mechanical compressors are needed, which are costly and usually have high energy demand.

Hydrogen at high pressure comes with safety issues. High pressure, high purity hydrogen at room temperature has significant effects on the mechanical properties of metals. This phenomenon is known as high pressure hydrogen embrittlement [33]. Mechanical failure or damage of high-pressure hydrogen storage devices can results in a jet that is easily flammable. Jet release in a confined or congested area can create an explosion hazard [34].

Despite the safety issues, high-pressure hydrogen storage is fairly popular thanks to its quick refill time and it offers the simplest solution in terms of infrastructure. Fast filling however, comes with an increase in temperature, which reduces the storage capacity once the temperature settles down again [33]. Therefore, even for a highly developed and mature hydrogen storage technique, research is still needed to optimize storage capacity and mitigate risks.

Cryogenic Liquid

Cryogenic storage of hydrogen requires the gas to be cooled down to -253°C, this process is both time consuming and energy intensive. Up to 40% of the energy content can be lost [35].

In liquefied hydrogen storage, hydrogen density goes well above 70 g/L [29] [36]. This is the main advantage of cryogenic liquid hydrogen storage. Cryogenic hydrogen storage is mainly used in space programmes and dedicated ships and trucks for high amount of hydrogen transport.

Highly insulated vessels are required to keep the temperature from increasing and avoid hydrogen to exceed its boiling point (-252.77°C [20]). In the case of unstable austenitic stainless steels that are often used for cryogenic storage vessels, insulation is also needed to avoid cold embrittlement of brittle parts through the thermal conduction, especially when temperatures reach over -150°C [35].

Solid Metal-Hydride

Solid H_2-storage systems are key elements to assure the transition to H_2 economy and are presently the most challenging and demanding subject for

innovative research. Hydrogen stored in a solid-state at low pressure is a safer, more convenient method compared to high-pressure gas and cryogenic liquefaction technologies [37]. Compared to the volumetric energy density of gaseous (4.4 MJ/L) and cryogenic (8.4 MJ/L), metal-hydride can deliver an energy density of up to 13 MJ/L [38].

Solid Metal-Hydride storage uses the reversible chemical process of reaction between a crystal-structured solid metal with hydrogen gas. When hydrogen comes in contact with the surface of the metal, the hydrogen molecule splits into two separate hydrogen atoms that are absorbed into the crystal structure of the metal to create a metal-hydride, as is schematically represented in Figure 8.

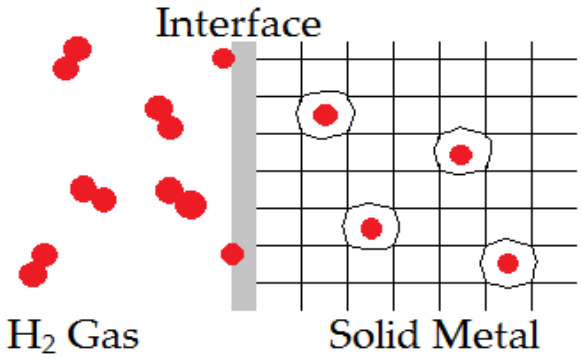

Figure 8: Schematic representation of Solid-Hydrogen Metal-Hydride storage technique.

The process of absorption is called the hydriding process, and heat is released as a result of the exothermic reaction happening. When heat is applied to the metal-hydride, the hydrogen is released as a gas. This process is called the de-hydriding process. Both the hydrogen and metal go back to their original phase and the reaction is therefore reversible according to the expression:

$$M + \frac{x}{2} H_2 \leftrightarrow MH_x + \Delta H \tag{23}$$

Where, M is the metal, H_x is the hydrogen that is hydrided by the metal, and ΔH is the amount of heat released or applied. The gas-solid phase equilibrium pressure (P_{eq}) is described by the van't Hoff's equation corrected by the hydrogen-to-metal ratio ($f(X)$) [39]:

$$\ln\left(\frac{P_{eq}}{P_0}\right) = \frac{\Delta H}{RT} - \frac{\Delta S}{R} + f(X) \quad (24)$$

Where P_{eq} is the equilibrium pressure of the Metal-Hydride, P_0 is the standard pressure (1.013 bar), ΔH is the enthalpy of formation in (J/mol H_2), and ΔS is the entropy of formation at standard pressure in (J/K·mol^{-1}).

The quantities ΔH and ΔS vary with alloy composition and have different values for absorption and desorption due to hysteresis. $f(X)$ is expressed by the following general form:

$$\mathrm{f(X)} = \sum_{i=1}^{9} a_i tan^i \pi(\frac{X}{X_{max}} - \frac{1}{2}) \quad (25)$$

Where, the coeffcients a_i are derived by regressing from the experimental data and are shown in Table 2.

Table 2: Values of the coeffcients a_i [39]

i	***a_i (des)***	***a_i (abs)***
1	1.7377126 x 10^{-1}	1.2315971 x 10^{-1}
2	3.3038405 x 10^{-3}	-7.8926198 x 10^{-3}
3	-5.5663079 x 10^{-2}	5.7950569 x 10^{-4}
4	5.1351774 x 10^{-2}	3.8577497 x 10^{-2}
5	19871619 x 10^{-2}	-1.2200087 x 10^{-2}
6	-2.3259416 x 10^{-2}	-1.7284550 x 10^{-2}
7	6.9099218 x 10^{-3}	5.1403940 x 10^{-3}
8	-8.8152755 x 10^{-4}	-6.3770055 x 10^{-4}
9	4.2083746 x 10^{-5}	-2.9345203 x 10^{-5}

The equilibrium pressure depends on the alloy used and at constant temperature, it can be found from the pressure-composite (P-C) isotherm. The P-C Isotherm is used to determine key characteristics of the material, such as the equilibrium pressure and maximum storage capacity [40] as displayed in Figure 9.

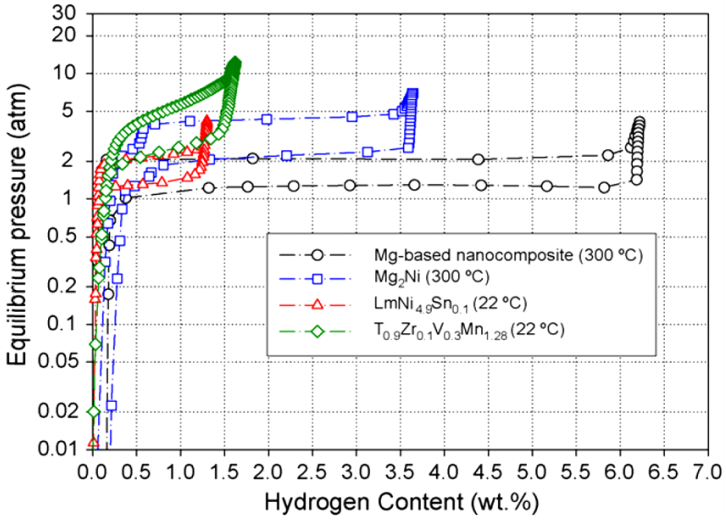

Figure 9: P-C Isotherm for various types of nano-materials for Solid-Hydrogen Energy Storage [37]

Energy may be needed to de-hydride the metal-hydride. Part of this energy will come from the heat generated by the exothermic reaction in the Fuel Cell itself, but additional energy is required to heat the metal-hydride sufficiently. This energy can result in so-called parasitic losses in the RHFC system and result in a slight increase of energy required from the Fuel Cell. To desorb 1 mol of Hydrogen, 75 kJ of energy is required. Knowing that 3.6 MJ is equal to 1 kWh of electricity, 0.03 kWh is required per mol of hydrogen desorbed.

As can be seen in Figure 9, storage capacity (in weight-percentage) and equilibrium pressure (in atm) vary based on the metal used. To optimize properties of the nano-structured metal, catalysts are added, either to reduce thermal energy required for de-hydriding or to increase the storage capacity.

Besides the material development, there are also main challenges in the development of metal-hydride storage containers. The aim is to achieve a compromise between the hydrogen storage density, integrity of the containment at the operating conditions and dynamic performance of hydrogen uptake and release. Manufacturability and lowering the costs are also very important factors to consider [35].The gas–solid equilibrium given by the van't Hoff equation is the basis for designing a hydride storage system.

The main energy demand occurs during hydrogen release. This energy demand is composed of three contributions: the heat required to heat the hydride up to desorption temperature, the heat of reaction and the work of compression to

reach the targeted outlet pressure [41].To optimize an integrated and limit parasitic losses due to thermal energy requirements, the selected metal-hydride pressure- and temperature characteristics should match the fuel cell operating temperature [42]. An overview of various metal-hydride storage techniques and their potential in different types of fuel cell can be found in Figure 10.

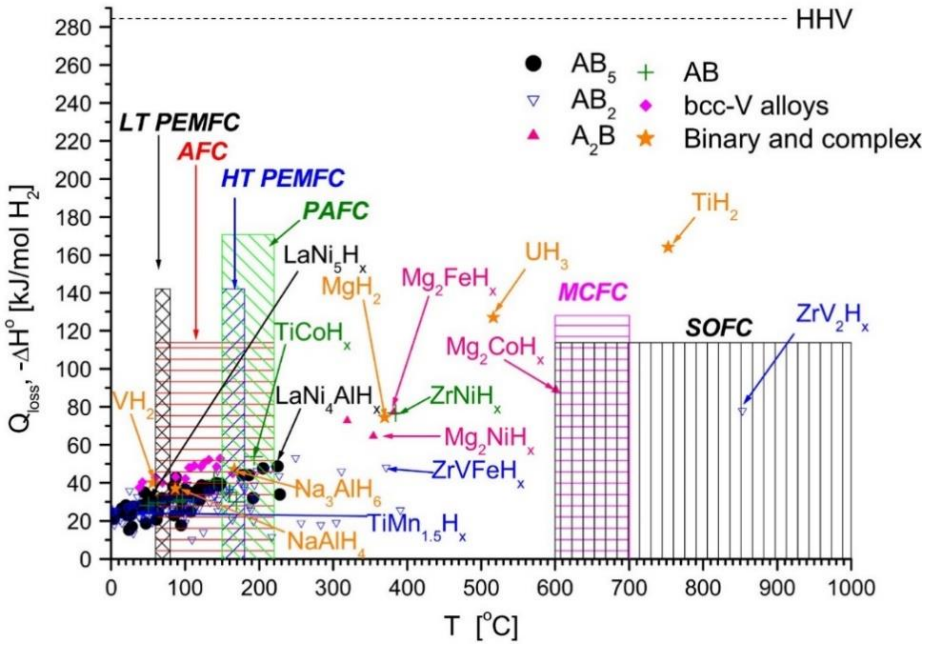

Figure 10: Potential of various Metal-Hydrides with the associated heat losses (Q_{loss}) in different types of fuel cells. The operation temperatures of the MH's correspond to H_2 plateau pressures of 10 bar [42]

Fuel Cell system

Fuel cells are electrochemical devices that combine oxygen and hydrogen to produce electricity. Since the invention of the fuel cell by William Robert Grove in 1838, it took a while for fuel cells to develop to commercial products. Nowadays, different technologies are avialbable as can be seen in Figure 10.

Fuel Cell Technologies

Different applications require different types of fuel cells and therefor progress is made in development of these technologies. Fuel cells are usually classified by the type of electrolyte used. The most common types of fuel cells using hydrogen as reactant are:

Alkaline Fuel Cell (AFC) is the oldest fuel cell technology and was used by NASA mid-1960 for space programs. The electrolyte used is an aqueous alkaline solution, such as potassium hydroxide (KOH).

Phosphoric Acid Fuel Cell (PAFC) uses phosphoric acid (H_3PO_4) as a liquid electrolyte solution. Hydrogen is used as a fuel and the hydrogen ion (H^+) migrates through the electrolyte to react with oxygen and electrons at the other side. The overall reaction in this fuel cell is similar to the PEMFC [43].

Molten Carbonite Fuel Cell (MCFC) operates at high temperatures of 600°C - 700°C. The electrolyte used is a molten alkali carbonate such as lithium or potassium-carbonate retained in a ceramic matrix of lithium aluminium oxide. Hydrogen combines with incoming carbonate ions (CO_3^{2-}) and produces carbon dioxide and water as by-products [43].

Solid Oxide Fuel Cell (SOFC) operates at high temperatures of 800°C – 1,000°C. The electrode is a solid ceramic based material like yttrium-stabilized zirconium (YSZ). It can operate with hydrogen fuels as well as with natural gas, biogas, coal gas etc. Here it is the oxygen that migrates through the electrolyte [43].

Polymer Electrolyte Membrane Fuel Cells (PEMFC) are the most widely used fuel cell technology. PEMFC's deliver high power density as well as low weight and volume compared to other fuel cells [44]. The PEMFC operates at low temperatures of 60-120ºC. Hydrogen is used as a fuel and the hydrogen ion (H^+) migrates through the electrolyte to react with oxygen and electrons at the other side.

Polymer Electrolyte Membrane Fuel Cell

A typical PEMFC consists of two electrodes; a positively charged cathode and a negatively charged anode, with in between the anode and cathode a polymer electrolyte membrane. Hydrogen is introduced in the anode side of the fuel cell; the electrolyte allows hydrogen protons to go through, but forces electrons to go around, creating an electrical current. Oxygen in the cathode side bonds with hydrogen to form water and heat.

Reactions happening in the catalyst layers of the PEMFC produce an electric potential difference between the electrodes. When both electrodes are isolated from each other and the electrolyte allows ionic mass transport, the electric potential difference can be used in an external circuit.

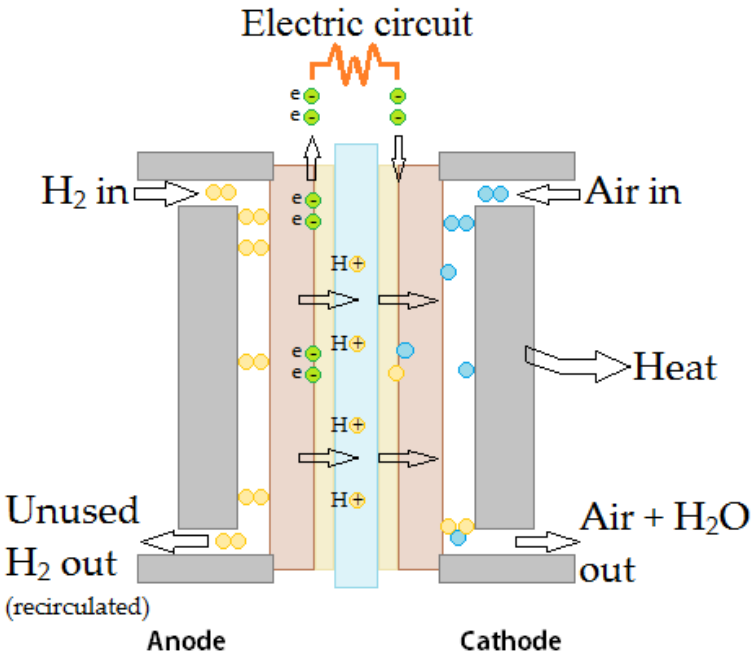

Figure 11: Schematic representation of a PEMFC

Figure 11 shows a schematic representation of the basic operation principles in a PEMFC. Hydrogen gas (H_2) comes in through the electrode (anode bipolar plate), it is then diffused through the Gas Diffusion Layer (GDL) before coming in contact with the Catalyst Layer (CL). In the anode CL, hydrogen oxidation occurs:

$$H_2 \rightarrow 2H^+ + 2e^- (Hydrogen\ Oxidation\ Reaction) \qquad (26)$$

When properly hydrated, the Polymer Electrolyte Membrane (PEM) offers protonic conductivity and conducts the hydrogen protons (H^+) to the cathode catalyst layer. The PEM offers electric isolation between anode and cathode, creating a potential difference between the electrodes. Hence, the free electrons are forced through an external electric circuit before making its way to the cathode CL.

On the cathode side, air is forced in through the electrode (cathode bipolar plate) and diffused through the GDL before entering the cathode CL. In the cathode CL, oxygen reduction occurs:

$$\frac{1}{2}O_2 + 2H^+ + 2e^- \rightarrow H_2O \ \ (Oxygen\ Reduction\ Reaction) \quad (27)$$

The overall reaction then becomes:

$$H_2 + \frac{1}{2}O_2 \rightarrow \ H_2O + Electricity + Heat \quad (28)$$

Like the PEM electrolyser, the amount of electricity and heat produced depends on the operating conditios of the PEM Fuel Cell. The PEM fuel cell consist of similar losses compared to the electrolyser, except in the fuel cell environment the voltage drops with increased current drawn:

$$V_{FC} = V_{Nernst} - E_{act} - E_{ohm} - E_{conc} \quad (29)$$

Where, $V_{FC}$is the fuel cell voltage (V), V_{Nernst} is the Nernst voltage (1.229V), E_{act} is the activation overpotential (V), E_{ohm} is the ohmic overpotential (V), and E_{conc} is the concentration overpotential.

The activation overpotential is found by:

$$E_{act} = -2.3\frac{RT}{\alpha F}\log(i_0) + \frac{RT}{\alpha F}\log(i) \quad (30)$$

Where, R is the universal gas constant (8,314 J kmole^{-1} K^{-1}), T is the operating temperature (K), α is the charge transfer coefficient, F is the Faraday's constant (96,485 A s mole^{-1}), i_0 is the exchange current density (A cm^{-2}), and i is the operating current density (A cm^{-2}).

The ohmicoverpotential is found by:

$$E_{ohm} = iR_i \quad (31)$$

Where, R_i is the cell internal resistance (Ω cm^{-2}). The concentration overpotential is found by:

$$E_{conc} = \frac{RT}{nF}\ln\left(\frac{i_L}{i_L - i}\right) \quad (32)$$

Where, n is the number of electrons exchanged, and i_L is the limiting current density (A cm^{-2}).

Control system

A micro-grid is a small power distribution system that generates, stores and supplies electricity in a decentralized environment and is seen as an important way to enable Sub-Saharan African countries to leap-frog traditional power generation systems and accelerate and improve electrification efforts [45]

In a smart micro-grid, the energy flow, information flow and business flow of the system and its application are integrated to be compatible with the Internet of Energy (IoE). The IoE is the innovative representation of the smart & connected energy systems. The aim of this technology is to promote a more flexible, personalized and efficient energy production that serves both the provider and the end-user of the energy. By strategically monitoring the energy big data, including energy generation, processing, transmission, distribution and consumption, the system allows this data to be used as a strategic resource to improve system performance through advanced ICT.

Where this study focusses on decentralized electricity generation, hydrogen storage and conversion is very well suitable for use in the IoE. With surplus electricity being converted into hydrogen, it is now possible to use this hydrogen not only for generation of electricity, but also other forms of energy such as cooking and space heating.

Levelised Cost of Electricity

The Levelised Cost of Electricity (LCOE) is an important financial parameter to measure cost-effectiveness of energy generating technologies. Although LCOE calculations are highly sensitive to the underlying data, it offers a comparison between projects and technologies.

LCOE aims to provide comparisons of different technologies with different project size, life time, different capital cost, return, risk, and capacities. It is an economic assessment of the total cost to build and operate a power-generating asset over its lifetime divided by the total energy output of the asset over that lifetime [46]. The LCOE is calculated by:

$$LCOE\ (\frac{\$}{kWh}) = \frac{\sum_{t=1}^{n} C_t + M_t + F_t\ (\$)}{\sum_{t=1}^{n} E_t\ \ (kWh)} \tag{33}$$

Which covers the whole lifetime of the energy system from year 1 ($t = 1$) to end of life ($t = n$). Where, C_t is the capital expenses (CAPEX), M_t are the

operation & maintenance expenses (OPEX), F_t are the fuel costs, and E_t is the electricity generated by the system.

As the lifetime of the technologies is often minimum 20 years, inflation rates should be taken into account as this influences the fuel and O&M costs over time. The lifecycle energy production strongly depends on the location of installation as solar irradiance and wind speeds vary strongly across the globe.

The system is sized to provide year-round electricity to the inhabitants without power outages due to the intermittence of the Solar PV and Wind energy sources. Three cases are studied for storage and back-up power for the micro-grid areanalysed: RHFC, Battery and Diesel generator (Genset). Finally, LCOE for a micro-grid entirely powered by a Genset is studied. The capital cost of the technologies used is presented in Table 3.

Table 3: Initial capital costs for selected technologies. Where applicable, a GBP – USD conversion factor of 1.406 is used.

Solar PV	$ 1,745.00	per $kW_{DC,peak}$	[47]
Wind Turbine	$ 1,406.00	per kW_{rated}	[48] [49]
Fuel Cell	$ 1,659.08	per kW_{rated}	[50]
Electrolyser	$ 1,321.64	per kW_{rated}	[51]
Hydrogen storage[1]	$ 468.20	per Kg H_2 stored	[52]
Diesel Generator	$ 913.90	per kW_{rated}	[53]
Diesel	$ 1.00	per Litre	[53]
Battery	$ 253.08	per kWh	[54]

Besides capital costs, costs for shipping, local taxes and import charges apply to deploy an energy system in Senegal as shown in Table 4. During operation, technologies efficiency drops due to wear of materials, contamination etc. With a long system lifetime, these degradations should be taken into account as they influence the system energy generation or capacity over time. The annual degradation rates for the used technologies are shown in Table 5.

[1] Storage cost target of DOE is 333 $/kg H_2, as technology is not mature yet, current costs are assumed based on experience to be 50% higher.

Table 4: Additional costs for deploying in Senegal

Cost per container	$ 2,390.20	[55]
Import charges	10%	[56]
VAT	18%	[56]

Table 5: Annual energy generation degradation rates

Solar PV degradation	0.50%	[57]
Wind Turbine degradation	1.60%	[58]
Fuel cell degradation	0.90%	[59]
Electrolyser degradation	0.90%	[59]
Battery degradation	1%	[60]
Diesel generator	1%	[61]

Operation and maintenance (O&M) costs are essential for LCOE calculations as they will increase costs over the lifetime and are affected by inflation rates. O&M costs of the analysed technologies are shown in Table 6.

Table 6: O&M costs for selected technologies

Solar PV	1.50%	of Capital cost	[62]
Wind Turbine	$ 70.30	per kW installed	[63]
Fuel Cell	$ 0.04	per operating hour	[64]
Electrolyser	$ 0.04	per operating hour	[64]
Battery	1%	of Capital cost	[65]
Storage tank	0.25%	of Capital cost	
Diesel generator	$ 1.10	per operating hour	[66]

Table 7 shows the assumed efficiencies for the simulations in order to determine the amount of energy produced and fuel required for the selected technologies where climate data is not sufficient.

Table 7: Assumed constant efficiencies for selected technologies

Battery round trip	92.5%	[65]
Diesel generator	21%	[67]
Converter	92 %	

The first case analysed is for a system with an RHFC back-up system. In this system, excess energy is sent to an electrolyser to convert water into hydrogen. The hydrogen is then stored in a Magnesium based metal-hydride for safe storage.

The second case analysed is for using a battery pack as back-up system. The battery size in ampere-hours (Ah) is calculated by:

$$C_n = \frac{E_L \cdot F}{MDOD \cdot TCF \cdot V_n} \tag{34}$$

Where $C_n$is the battery capacity (Ah), E_L the average daily load (kWh/day), F the days of storage required, $MDOD$ the maximum depth of discharge for the battery without damaging, TCF the temperature correction factor (vary with battery type, lower temperatures limit the maximum allowable depth of discharge), and V_n is the battery voltage output. Chosen is a Lithium-Ion battery because of the stability at higher temperatures in Senegal [68].

The third case analysed is this of a diesel generator back-up system. A diesel generator is common to use in Sub-Saharan Africa, despite the high fuel costs, noise and emissions.

A fourth case is added to see how the renewable energy micro-grid compares to a micro-grid based on fossil fuel energy generation using only a diesel generator. Even though it is common to have a small diesel generator per household in Sub-Saharan Africa, it is becoming more popular to buy a bigger diesel generator with a small community to share costs and profits and hence lower LCOE compared to the reported 42 cents per kWh for household diesel generators [53].

RESULTS

Renewable energy is widely available on the selected site as can be seen in Figure 4. The wind statistics require extra analysis to determine and predict the annual energy potential in the wind. From equation 7 to 15, the wind speed distribution is found to be Weibull by plotting the wind speed distribution against

both Weibull and Rayleigh wind probability functions as shown in Figure 12. Weibull wind distribution gives a wind power density of maximum 17 W/m^2 at 10m height as is shown in

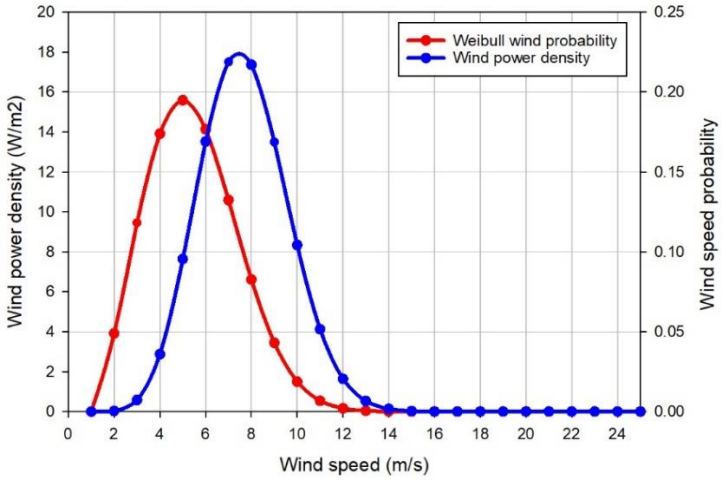

Figure 13. The mean wind speed is found to be 6.04 m/s at 40 meter height.

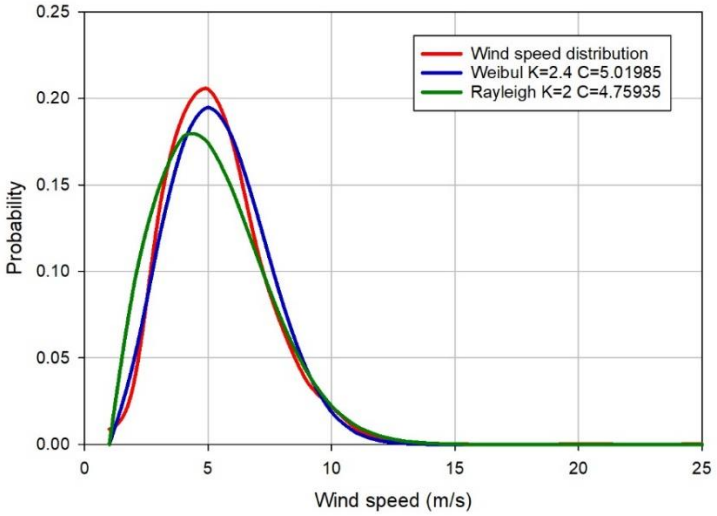

Figure 12: Weibull and Rayleigh wind probability functions and wind speed distribution

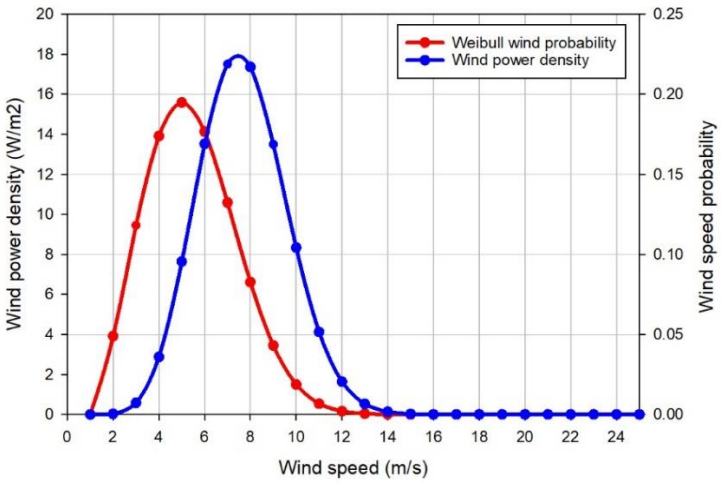

Figure 13: Weibull wind probability and wind power density (W/m^2).

The selected wind turbine power curve is plotted against the power available in the wind. The Cp of the wind turbine is plotted and shows the variance of Cp, peaking at 0.49 at rated power (10 m/s). Cut-in windspeed of the wind turbine is at 3 m/s while the cut-out windspeed is 25 m/s to protect from damage due to excessive winds. The wind turbine is rated at 10 m/s at 7kW and has an area of 18.86 m^2.

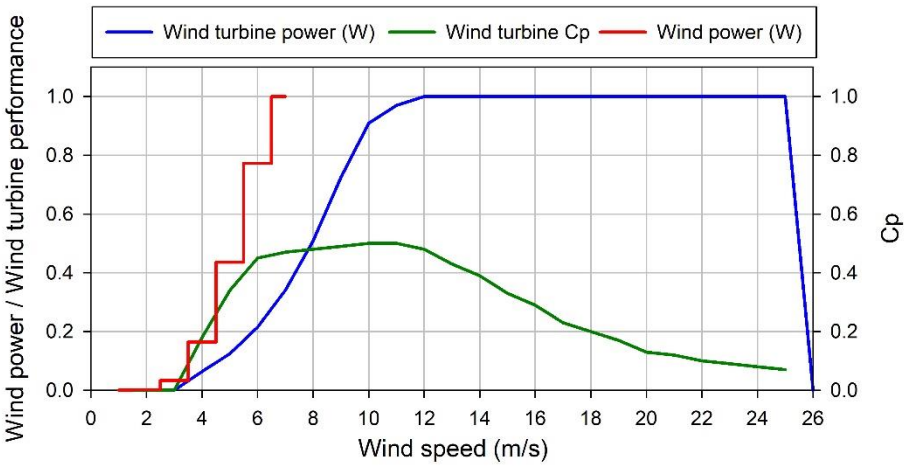

Figure 14: Cumulative Weibull wind probability, wind turbine power curve and wind turbine Cp

The integrated system is modelled in MATLAB/Simulink to verify its ability to follow the load of the micro-grid. Figure 15 shows the integrated hybrid renewable energy micro-grid system.

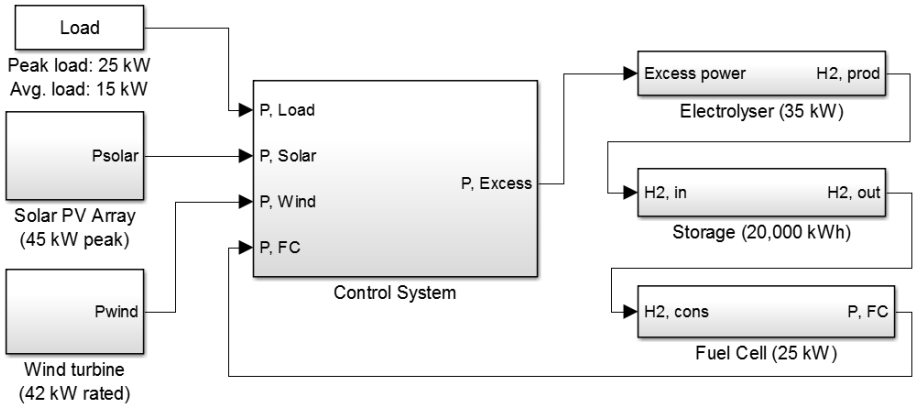

Figure 15: MATLAB/Simulink of the integrated hybrid renewable energy micro-grid system. The control system recognizes the energy generated Installed capacities are adjustable, values used for simulation of the micro-grid are shown above.

Using an iterative process, the optimum storage capacity was found to be 20,000 kWh of hydrogen stored. As shown in Figure 19, this gives sufficient amount of storage to have hydrogen available at all time during the year. Based on the lower heating value of hydrogen (120 MJ/kg = 33.33 kWh/kg), the amount of hydrogen stored is then 600.06 kg. Table 8 shows the system sizing data.

Table 8: System input sizing data

System lifetime	20	yrs	[69]
Inflation rate	2.3	%	[70]
Installed capacity PV	45	kW_{peak}	
Installed capacity wind	42	kW_{rated}	
Installed capacity FC	25	kW_{rated}	
Installed capacity Storage	600.06	Kg H_2	
Installed capacity EL	35	kW_{rated}	
Installed capacity Genset	25	kW_{rated}	

The electrolyser is powered directly from the excess energy of renewables, therefore the operating conditions are constantly changing. A similar trend occurs for the PEM Fuel Cell, as the technologies are modelled in similar ways. The conversion efficiency varies over the operating range as can be seen in Figure 16.

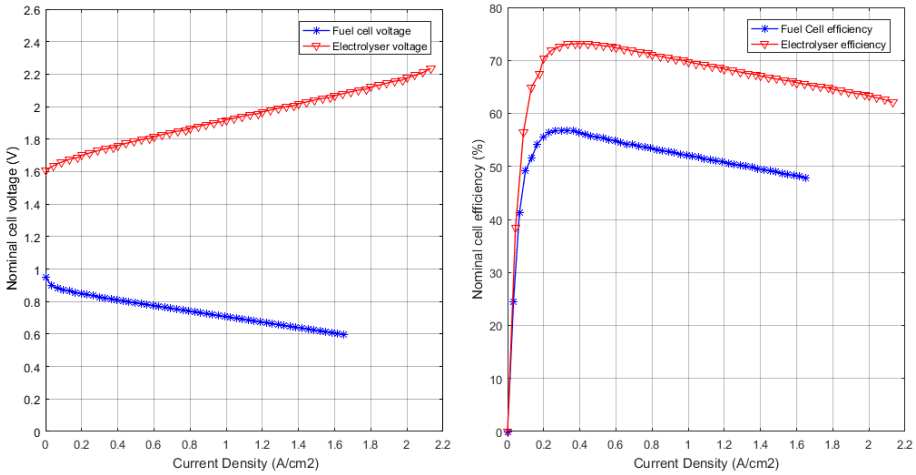

Figure 16: Efficiency and voltage characteristics of the PEM Electrolyser and PEM Fuel Cell as a function of current density (A/cm^2)

The metal-hydride used in the Solid-Hydrogen Storage Cell is $Ti_{0.95}Zr_{0.05}V_{0.2}Mn_{1.3}$. The AB2 Ti-based alloys have great potential sorption capacity at ambient temperature (~2 H-wt.%) with high reactivity rates. Figure 13 shows the desorption rate of $Ti_{0.95}Zr_{0.05}V_{0.2}Mn_{1.3}$, showing the ability to discharge instantaneous and at a much higher rate than $LmNi_{4.9}Sn_{0.1}$, providing better load-following capabilities.

Figure 17 shows the storage capacity of $Ti_{0.95}Zr_{0.05}V_{0.2}Mn_{1.3}$. From experimental studies, the maximum storage capacity of 2 H-wt.% is initially achieved, but only during the activiation of the material . Hereafter, the maximum storage capacity drops to around 1.6 H-wt.% and stays stable [71].

Figure 18 shows the desorption rate of $Ti_{0.95}Zr_{0.05}V_{0.2}Mn_{1.3}$. With 600.06 kg (equal to 20,000 kWh) H_2 stored and a storage capacity of 1.6 wt.%, the total amount of Ti-based alloy in the storage system is 33,500 kg. With an instantaneous desorption of 30 cc/min/g, the total amount of hydrogen discharged based on the installed storage capacity and assuming all hydrogen storage cells discharge simultaneously is 100,000 L/min. The maximum flow rate towards the fuel cell, at maximum power of 25kW, is 38.8 L/min. Therefore, it is possible to devide the Ti-based alloy over multiple storage cells for optimized thermal management.

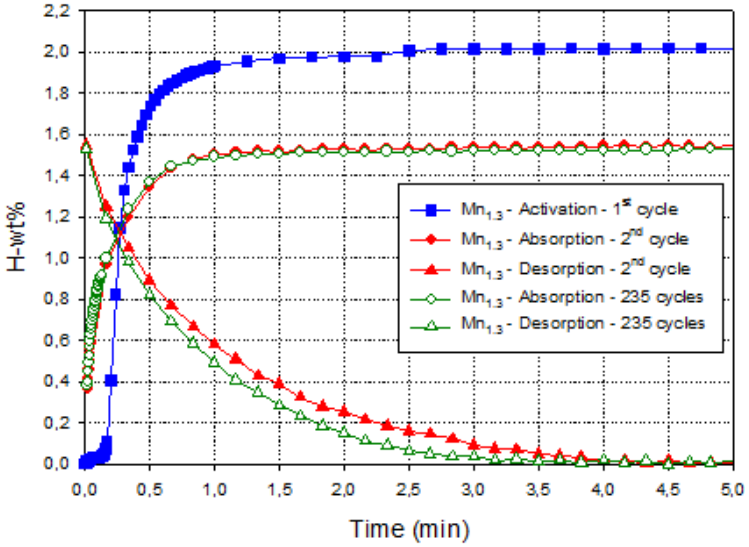

Figure 17: Dynamic measurements for $Ti_{0.95}Zr_{0.05}V_{0.2}Mn_{1.3}$ alloy taken during activation, after 2 and after 235 cycles [71].

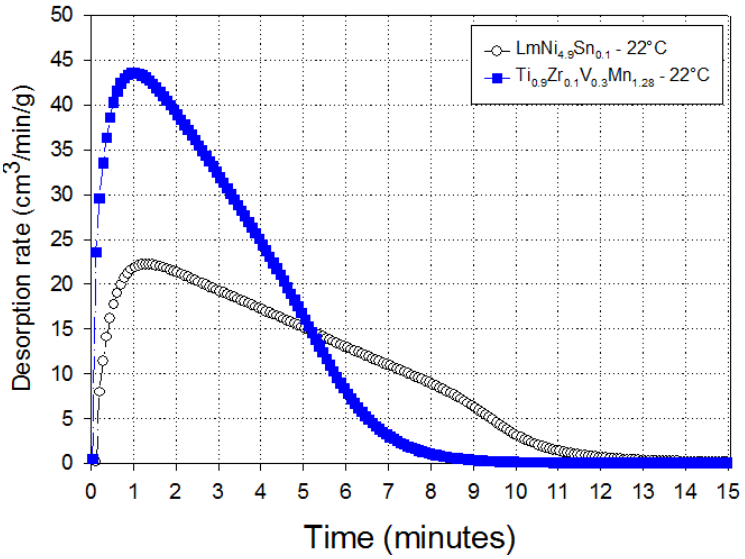

Figure 18: Desorption rate comparison for $LmNi_{4.9}Sn_{0.1}$ and $Ti_{0.95}Zr_{0.05}V_{0.2}Mn_{1.3}$ [71].

Figure 19 shows the hydrogen state-of-charge throughout the year. It can be seen that excess energy during the first half year is sufficient to provide seasonal shifting of this energy and use this during the second half of the year. Seasonal shifting is one of the advantages of hydrogen storage over conventional lithium-ion battery storage, as there is neglectable self-discharge of the storage system.

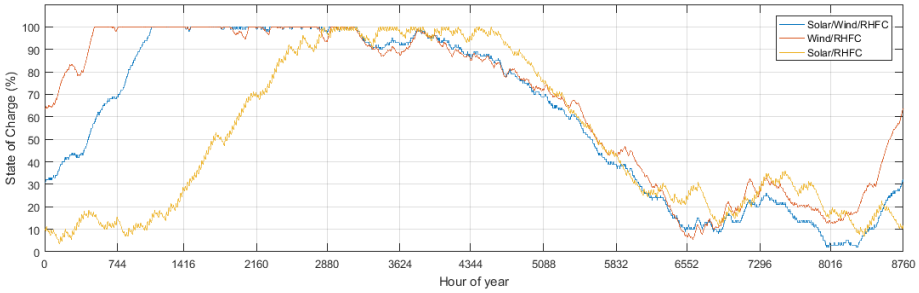

Figure 19: Hydrogen State-of-Charge throughout the year. The hydrogen SOC, consumption and production in the month of October (period C) is shown in Figure 20. Detailed representation of the systems performance in week A and B are shown in Figure 21. The storage SOC at T=0 is equal to the SOC at T=8760 to show the ability to recharge to 100% in the following year.

Figure 19 shows the Sate-of-Charge of the Solar PV/Wind energy system compared to that of system consisting of only one renewable energy source, either Solar PV or Wind.

Table 9 shows the operating details of the system. Since solar energy is only available during daytime, reducing the amount of operating hours of the electrolyser while increasing the operating hours of the fuel cell. This means more hydrogen needs to be produced in a shorter amount of time, hence increasing the installed capacities of both the Solar PV and electrolyser in order to produce adequate hydrogen. Wind energy is more available as can be seen in Figure 4, especially in the months December – March. Combining both renewable energy technologies into one system optimizes the LCOE further, hence this configuration is further analysed and compared to alternative energy storage and back-up systems.

Table 9: Comparison of energy systems with RHFC back-up

	Solar/RHFC	Wind/RHFC	Solar/Wind/RHFC
Solar PV			
- Installed capacity	187 kW	N/A	45 kW
- Capacity factor	15.79%	N/A	15.79%
Wind			
- Installed capacity	N/A	78 kW	42 kW
- Capacity factor	N/A	36.50%	38.52%
Electrolyser			
- Installed capacity	150 kW	50 kW	35 kW
- Operating hours	2,978	4,860	5,028
- Average efficiency	66.39%	66.15%	66.33%
Storage			
- Installed capacity	20,000 kWh	20,000 kWh	20,000 kWh
Fuel Cell			
- Installed capacity	25 kW	25 kW	25 kW
- Operating hours	5,782	3,900	3,732
- Average efficiency	46.97%	49.15%	49.63%
LCOE (¢/kWh)	**10.48**	**10.27**	**10.18**

Figure 20 zooms in on the hydrogen charge and discharge over the month of August. Here it shows the RHFC switching from charge to discharge mode several times depending on the availability of renewables, and the effect on the hydrogen state of charge.

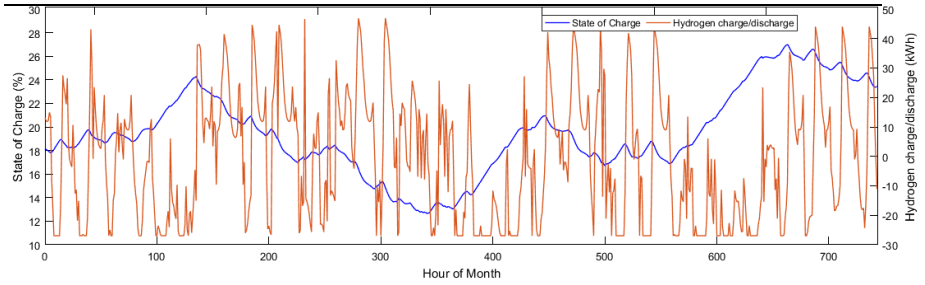

Figure 20: Hydrogen production, consumption and state of charge during October. Here, a negative value for the hydrogen charge/discharge means hydrogen is being produced and stored, whereas a positive value means it is discharged and converted into electricity.

Figure 21 shows two simulation weeks. During week A, from 15 – 21 March, Wind and Solar PV generate plenty excess energy to recharge the hydrogen reservoirs. During this week, the load is mainly powered by renewables and the fuel cell is barely required as a back-up. Therefore, the reservoir will be recharged for periods with less renewable energy available such as in week B. Week B (9 – 15 September), is a period with low renewable energy generation. During the day, some Solar PV is available to power the load, but Wind energy is lacking. Therefore, the fuel cell is required to power the load. This can be seen in a depletion of the hydrogen storage reservoir, whose state-of-charge drops significantly during this week. Week A also shows the electrolyser reaching its maximum capacity while not all excess energy is used. These periods of the year occur, however not often enough to benefit a larger capacity electrolyser. Excess energy that cannot be used by the electrolyser can be used for extra load, for example powering extra households or future extension of the micro-grid.

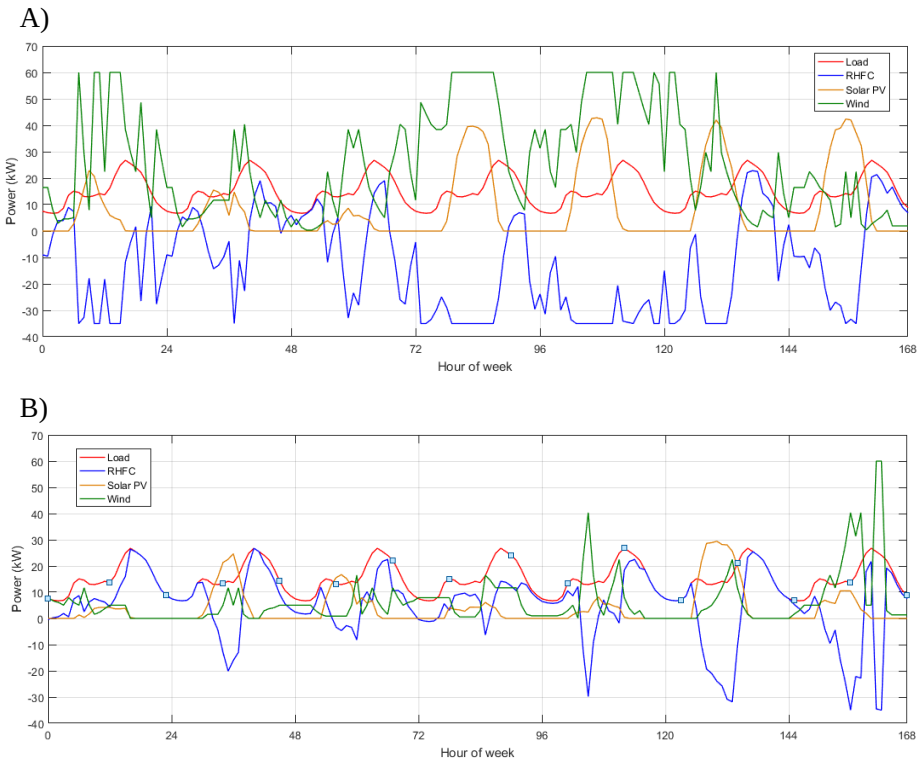

Figure 21: MATLAB/Simulink simulation results for the weeks of A) 15 – 21 March and B) 9 – 15 September. When renewable energy is available, this is send to power the load. When there is an excess of renewable energy generated, this is send to the electrolyser to produce hydrogen (H_2), as is visible when the hydrogen charge is represented by a 'negative discharge' of the Solid-Hydrogen Energy Storage modules. When renewable energy generation is not sufficient to power the load, the PEM Fuel Cell covers the load requirements.

Zooming in on a a short period of two days, it can be seen in Figure 22 that the fuel cell successfully follows the load when there is no energy available from renewable sources. The smart control system recognizes when electricity is generated by the renewables. In this case, the fuel cell will be tuned down so that the renewables have priority in powering the load. This is done for two reasons. First, this allows to keep hydrogen storage charged in case of emergencies and second, the electricity from renewables is cheaper per unit (¢/kWh) and therefore

the load is always powered by the most cost effective source of electricity available.

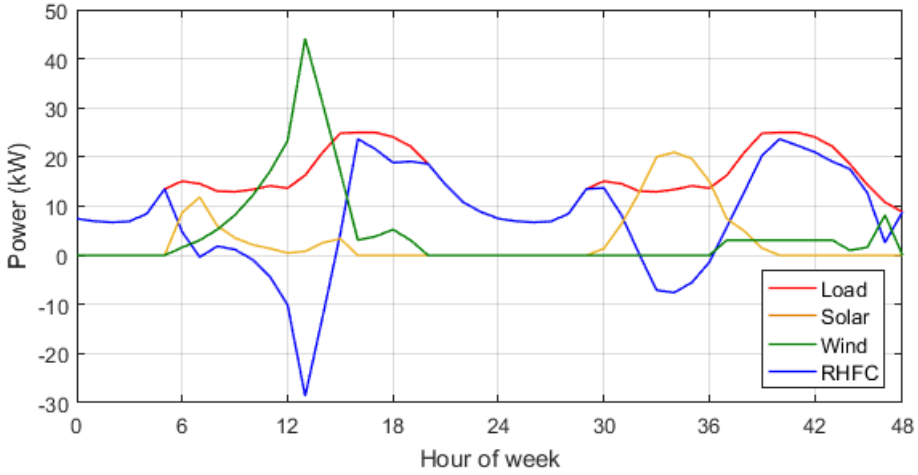

Figure 22: Zoom-in on load-following RHFC on 27 and 28 September

The annual energy flow in the system is shown in Figure 23. Here it is seen that theoretically all hydrogen molecules in the Fuel Cell react and form water which can be used as feedstock to the electrolyser. This water contains thermal energy that can be used to reduce parasitic losses occurring due to dehydriding the metal-hydride and pre-heating water for electrolysis.

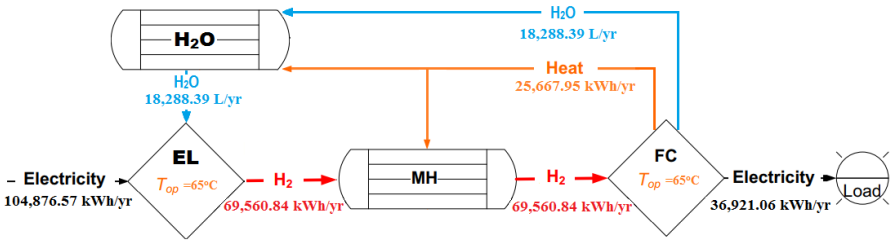

Figure 23: Schematic of annual energy flow in the RHFC system

The RHFC backup is compared to identical renewable energy systems with a diesel genset and battery as backup technologies, and to a stand-alone diesel genset energy system as is shown in Table 10 and Figure 24. As a back-up system for this configuration, the RHFC provides the lowest LCOE in combination with the PV/Wind system. Despite the high capital cost of the RHFC, the long lifetime

provides a lower LCOE due to the amount of energy delivered over its lifetime Also its operation and maintenance cost are low, and because of its low maintenance requirements. Simplified fuel logistics and reduced site-visits further benefit the autonomous system for rural communities.

Table 10: Levelised Cost of Electricity (¢/kWh) for 25kW small micro-grid near Dakar, Senegal

	PV/Wind/ RHFC	**PV/Wind/ Battery**	**PV/Wind/ Genset**	**Genset**
Capital cost	6.75	14.85	2.04	0.20
O&M	1.50	4.46	2.54	1.97
Fuel cost	-	-	7.30	16.10
Import	0.77	1.48	0.20	0.02
VAT	1.07	2.67	0.37	0.04
Shipping	0.07	0.09	0.06	0.02
Total	**10.17**	**23.56**	**12.51**	**18.35**

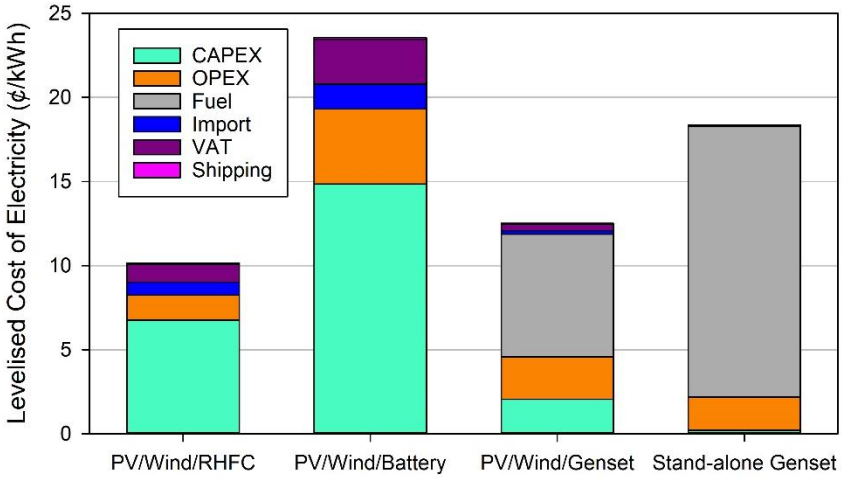

Figure 24: Levelised Cost of Electricity (¢/kWh) for 25kW small micro-grid near Dakar, Senegal

CONCLUSION

An autonomous renewable energy generating and back-up system is proposed and successfully validated using MATLAB/Simulink and experimental testing of individual components and the integrated system. The system provides

the full load requirements of the cell phone tower throughout the year and can be scaled accordingly to provide electricity for small communities near the cell phone tower.

The optimized energy system consist of 45 kW Solar PV arrays, 42 kW Wind Turbines for renewable power generation, assisted by a 35kW PEM electrolyser to convert excess electricity into hydrogen, a 20,000 kWh of hydrogen stored in AB2 Ti-based alloy and a 25kW PEM Fuel Cell to regenerate electricity in absence of renewable energy sources.

LCOE calculations based on the outcomes of the MATLAB/Simulink model show the economic potential of an RHFC as back-up for micro-grids, allowing cheap and reliable electricity to rural areas in developing countries, with a LCOE of 10.17 ¢/kWh, RHFC is the most cost efficient back-up for this application.

However, the system is highly influenced by local climate, hence the LCOE and system sizing should be individually configured based on the geographical location of the planned deployment.

Acknowlegdement

This study is sponsored by and carried out in collaboration with SolarBotanic Ltd.

REFERENCES

[1] World Economic Forum, "The Global Risks Report 2018," World Economic Forum, Geneva, 2018.

[2] REN21, "Renewables 2017 Global Status Report," REN21 Secretariat, Paris, 2017.

[3] Bloomberg New Energy Finance, "New Energy Outlook 2017," Bloomberg Finance L.P., London, 2017.

[4] NREL, "Overgeneration from Solar Energy in California: A Field Guide to the Duck Chart," National Renewable Energy Laboratory, Golden, CO, 2015.

[5] California ISO, "What the duck curve tells us about managing a green grid," 2016. [Online]. Available: https://www.caiso.com/Documents/FlexibleResourcesHelpRenewables_FastFacts.pdf. [Accessed 31 01 2018].

[6] International Energy Agency, "Energy Access Outlook 2017," 19 10 2017. [Online]. Available: https://www.iea.org/access2017/. [Accessed 11 01 2018].

[7] A. Vaccaro, R. Baseil, H. Hagras, M. Ho, P. Krein, R. Larsen, Glenn McKnight, V. Modi, A. E. Pascual, K. Passino, K. Perusich and A. Zobaa, "Reliable Electric Power for Developing Countries," Humanitarian Technology Challenge, In Press.

[8] H. K. Chavula, "Telecommunications development and economic growth in Africa," *Information Technology for Development* , vol. 19, no. 1, pp. 5-23, 2013.

[9] GSMA, "Tower Power Africa," GSMA, 2014.

[10] L. Graves, "Energy priorities and strategies for Africa's 'Big Four' towercos," 02 05 2017. [Online]. Available: https://www.towerxchange.com/energy-priorities-and-strategies-for-africas-big-four-towercos/. [Accessed 08 06 2016].

[11] GSMA, "Powering Telecoms: West Africa Market Analysis," GSMA, London, 2013.

[12] REA, "Development of decentralised energy and storage systems in the UK," KPMG, 2016.

[13] R. Swami, "Solar Cell," *International Journal of Scientific and Research Publications*, vol. 2, no. 7, 2012.

[14] R. Baños, F. Manzano-Agugliaro, F. Montoya, C. Gil, A. Alcayde and J. Gómez, "Optimization methods applied to renewable and sustainable energy: A review," *Renewable and Sustainable Energy Reviews*, vol. 15, no. 4, pp. 1753-1766, 2011.

[15] SERI, Basic Photovoltaic Principles and Methods, Golden: Technical Information Office, 1982.

[16] D. Y. Goswami and F. Kreith, "Photovoltaics Fundamentals, Technology and Application," in *Handbook of Energy Efficiency and Renewable Energy*, Boca Raton, Taylor & Francis Group, 2007.

[17] D. Vatansever, E. Siores and T. Shah, "Alternative Resources for Renewable Energy: Piezoelectric and Photovoltaic Smart Structures," in *Global Warming - Impacts and Future Perspective*, P. D. B. R. S. (Ed.), Ed., InTech, 2012.

[18] X. H. Nguyen and M. P. Nguyen, "Mathematical modeling of photovoltaic cell/module/arrays with tags in Matlab/Simulink," *Environmental Systems Research,* vol. 4, no. 24, p. Open Access, 2015.

[19] Los Alamos National Laboratory, "Periodic Table of Elements: LANL," 2016. [Online]. Available: http://periodic.lanl.gov/1.shtml. [Accessed 04 07 2016].

[20] T. Ghosh and M. Prelas, Energy Resources and Systems: Volume 2: Renewable Resources, 2 ed., Dordrecht: Springer Science+Business Media B.V., 2011.

[21] J. Xu and G. F. Froment, "Methane Steam Reforming, Methanation and Water-Gas Shift: 1. Intrinsic Kinetics," *AIChE Journal,* vol. 35, no. 1, pp. 88-96, 1989.

[22] "Marcelo Carmo; David L. Fritz; Jurgen Mergel; Detlef Stolten," *International Journal of Hydrogen Energy,* vol. 38, pp. 4901-4934, 2013.

[23] DOE Hydorgen and Fuel Cells Program, "Policies and Acts," 2015. [Online]. Available: https://energy.gov/eere/fuelcells/doe-technical-targets-hydrogen-production-electrolysis. [Accessed 21 09 2017].

[24] S. Ghandehariun and A. Kumar, "Life cycle assessment of wind-based hydrogen production in Western Canada," *International Journal of Hydrogen Energy,* vol. 41, no. 22, pp. 9696-9704, 2016.

[25] I. Vincent and D. Bessarabov, "Low cost hydrogen production by anion exchange membrane electrolysis: A review," *Renewable and Sustainable Energy Reviews,* vol. 81, pp. 1690-1704, 2018.

[26] A. Buttler and H. Spliethoff, "Current status of water electrolysis for energy storage, grid balancing and sector coupling via power-to-gas and power-to-liquids: A review," *Renewable and Sustainable Energy Reviews,* pp. 2440-2454, 2018.

[27] R. Bhandari, C. A. Trudewind and P. Zapp, "Life cycle assessment of hydrogen production via electrolysis – a review," *Journal of Cleaner Production,* vol. 85, pp. 151-163, 2014.

[28] J. Turner, G. Sverdrup, M. K. Mann, P.-C. Maness, B. Kroposki, M. Ghirardi, R. J. Evans and D. Blake, "Renewable hydrogen production," *International Journal of Energy Research,* vol. 32, no. 5, pp. 379-407, 2007.

[29] R. Gupta, Hydrogen Fuel: Production, Transport, and Storage, CRC Press, 2008.

[30] A. R. A. B. O. F. Andreas Züttel, "Hydrogen: the future energy carrier," *Philosophical Transactions of The Royal Society*, vol. 368, pp. 3329-3342, 2010.

[31] T. S. F. Jinsong Zhang, P. V. Ramachandran, J. P. Gore and I. Mudawar, "A Review of Heat Transfer Issues in Hydrogen Storage Technologies," *Journal of Heat Transfer*, vol. 127, no. 12, pp. 1391-1399, 2005.

[32] L. Klebanoff, Hydrogen Storage Technology: Materials and Applications, Boca Raton: CRC Press, 2013.

[33] J. Zheng, X. Liu, P. Xu, P. Liu, Y. Zhao and J. Yang, "Development of high pressure gaseous hydrogen storage technologies," *International Journal of Hydrogen Energy*, vol. 37, no. 1, pp. 1048-1057, 2012.

[34] L. Shirvill, T. Roberts, M. Royle, D. Willoughby and T. Gautier, "Safety studies on high-pressure hydrogen vehicle refuelling stations: Releases into a simulated high-pressure dispensing area," *International Journal of Hydrogen Energy*, vol. 37, pp. 6949-6964, 2012.

[35] H. Barthelemy, M. Weber and F. Barbier, "Hydrogen storage: Recent improvements and industrial perspectives," *International Journal of Hydrogen Energy*, vol. 42, no. 11, pp. 7254-7262, 2017.

[36] Y. Zhang, A. Smirnova, A. Verma and R. Pitchumani, "Design of a proton exchange membrane (PEM) fuel cell with variable catalyst loading," *Journal of Power Sources*, vol. 291, pp. 46-57, 2015.

[37] N. Rusman and M. Dahari, "A review on the current progress of metal hydrides material for solid-state hydrogen storage applications," *International Journal of Hydrogen Energy*, vol. 41, pp. 12108-12126, 2016.

[38] Z. Dehouche and N. Grimard, "NANOCOMPOSITE MATERIALS FOR HYDROGEN STORAGE," in *New Nanotechnology Research*, Gauthier, Nova Science Publishers, Inc., 2006, pp. 2-64.

[39] Z. Dehouche, W. d. Jong, E. Willers, A. Isselhorst and M.Groll, "Modelling and simulation of heating/air-conditioning systems using

the multi-hydride-thermal-wave concept," *Applied Thermal Engineering*, vol. 18, no. 6, pp. 457-480, 1998.

[40] A. Borgschutte, S. Kato, M. Bielmann and A. Zuttel, "Experimental Techniques to Measure of the Equiilibrium Plateua Pressures of Metal Hydrides," in *Proceedings of the International Symposium*, Richmond, 2009.

[41] K. M. W. A. Patrick Adametz, "Energetic evaluation of hydrogen storage in metal hydrides," *INTERNATIONAL JOURNAL OF ENERGY RESEARCH*, vol. 40, pp. 1820-1831, 2016.

[42] M. V. Lototskyy, I. Tolj, L. Pickering, C. Sita, F. Barbir and V. Yartys, "The use of metal hydrides in fuel cell applications," *Progress in Natural Science: Materials International*, vol. 27, no. 1, pp. 3-20, 2017.

[43] S. T. Revankar and P. Majumdar, Fuel Cells: Principles, Design, and Analysis, Boca Raton: CRC Press, 2014.

[44] Energy.gov, "www.energy.gov," 2016. [Online]. Available: http://energy.gov/eere/fuelcells/types-fuel-cells. [Accessed 31 05 2016].

[45] M. B. M. H. D. D. D. E. G. S. L. J. A. K. D. G. V. M. B. A. B.-H. K. Y. Manuel Welsch, "Smart and Just Grids for sub-Saharan Africa: Exploring options," *Renewable and Sustainable Energy Reviews*, vol. 20, pp. 336-352, 2013.

[46] C. S. Lai and M. D. McCulloch, "Levelized cost of electricity for solar photovoltaic and electrical energy storage," *Applied Energy*, vol. 190, pp. 191-203, 2017.

[47] Department of Energy & Climate Change, "Solar PV cost data," 26 05 2016. [Online]. Available: https://www.gov.uk/government/statistics/solar-pv-cost-data. [Accessed 2017 04 2017].

[48] M. Ragheb, "The Economics of Wind Energy," M. Ragheb, Illinois, 2017.

[49] IRENA, "The power of change: Solar and Wind cost reduction potential to 2025," International Renewable Energy Agency, Abu Dhabi, 2016.

[50] J. S. A. W. D. P. Jason Marcinkoski, "DOE Hydrogen and Fuel Cells Program Record," U.S. Department of Energy, 2015.

[51] Strategic Analysis Inc. & NREL, "Techno-economic Analysis of PEM Electrolysis for Hydrogen Production," 27 02 2014. [Online]. Available: https://energy.gov/sites/prod/files/2014/08/f18/fcto_2014_electrolytic_h2_wkshp_colella1.pdf. [Accessed 26 04 2017].

[52] DOE, "Hydrogen Storage," 2017. [Online]. Available: https://energy.gov/eere/fuelcells/hydrogen-storage. [Accessed 27 04 2017].

[53] S. Baurzhan and G. P. Jenkins, "Off-grid solar PV: Is it an affordable or appropriate solution for rural electrification in Sub-Saharan African countries," *Renewable and Sustainable Energy Review*, vol. 60, pp. 1405-1418, 2016.

[54] M. K.-M. P. B. C. J. V Viswanathan, "National Assessment of Energy Storage for Grid Balancing and Arbitrage," U.S. Department of Energy, Oak Ridge, 2013.

[55] FastLane, "Container Shipping To Senegal from UK," 2017. [Online]. Available: http://www.fastlanefwd.co.uk/FCL_and_LCL_Container_Shipping_Senegal.html. [Accessed 04 27 2017].

[56] Nations Ecyclopedia, "Senegal - Customs and duties," 2017. [Online]. Available: http://www.nationsencyclopedia.com/Africa/Senegal-CUSTOMS-AND-DUTIES.html. [Accessed 04 27 2017].

[57] Sunpower, "SunPower® X-Series Residential Solar Panels," 2017. [Online]. Available: https://us.sunpower.com/sites/sunpower/files/media-library/data-sheets/ds-x22-series-360-residential-solar-panels.pdf. [Accessed 04 25 2017].

[58] I. Staffell and R. Green, "How does wind farm performance decline with age?," *Renewable Energy*, vol. 66, pp. 775-786, 2014.

[59] H. D. C. A. G. S. Jennifer Kurtz, "V.F.10 Fuel Cell Technology Status—Degradation," in *FY 2015 Annual Progress Report*, Golden, DOE, 2015, pp. 174-179.

[60] NREL, "Backup Power Cost of Ownership Analysis and Incumbent Technology Comparison," National Renewable Energy Laboratory, 2014.

[61] S. Baurzhan and G. Jenkins, "On-Grid Solar PV versus Diesel Electricity Generation in Sub-Saharan Africa: Economics and GHG Emissions," *Sustainability*, vol. 9, no. 372, pp. 1-15, 2017.

[62] NREL, "Distributed Generation Renewable Energy Estimate of Costs," 02 2016. [Online]. Available: http://www.nrel.gov/analysis/tech_lcoe_re_cost_est.html. [Accessed 25 04 2017].

[63] NREL, "Cost and Performance Assumptions for Modeling Electricity Generation Technologies," National Renewable Energy Laboratory, Golden, 2010.

[64] I. T. Ender Ozden, "PEM fuel cell degradation effects on the performance of a stand-alone solar energy system," *International Journal of Hydrogen Energy*, vol. In Press, pp. 1-9, 2017.

[65] Lazard, "Lazard's levelized cost of energy storage - version 1.0," Lazard, 2015.

[66] HOMER, "HOMER Energy Report," 20 07 2016. [Online]. Available: http://usersupport.homerenergy.com/customer/en/portal/articles/2188634-diesel-o-m-costs. [Accessed 24 04 2017].

[67] NREL, "Backup Power Cost of Ownership Analysis and Incumbent Technology Comparison," National Renewable Energy Laboratory, Golden, 2014.

[68] AllCell Technologies LLC, "A Comparison of Lead Acid to Lithium-ion in Stationary Storage Applications," AllCell Technologies LLC, 2012.

[69] NREL, "Distributed Generation Renewable Energy Estimate of Costs," National Renewable Energy Laboratory, 02 2016. [Online]. Available: http://www.nrel.gov/analysis/tech_lcoe_re_cost_est.html. [Accessed 17 04 2017].

[70] Bank of England, "Inflation Report," Bank of England, London, 2017.

[71] M. S. F. L. J. G. Z. Dehouche, "Ti–V–Mn based alloys for hydrogen compression system," *Journal of Alloys and Compounds*, vol. 400, pp. 276-280, 2005.